Quantitative Analysis of Cytoskeletal Organization by Digital Fluorescent Microscopy

Nurit Lichtenstein, Benjamin Geiger, and Zvi Kam*
Weizmann Institute of Science, Department of Molecular Cell Biology, Rehovot, Israel

Received 21 July 2002; Revision received 2 March 2003; Accepted 11 March 2003

Background: The cytoskeleton consists of complex arrays of fibers that play indispensable roles in cell structure and function. The cytoskeletal fibers are concertedly involved in numerous cellular processes, including cell adhesion, locomotion, intracellular transport, and cell division. The organization of the cytoskeleton was extensively studied, mainly by immunofluorescence microscopy, yet these studies were mostly qualitative, and a reliable quantitative approach for determining fiber structure and distribution is still missing.
Methods: In this study we developed algorithms for filament feature extraction, based on fluorescence microscopy. These algorithms are robust against blurring by slight defocus, high background, and noise, and are applicable to both fixed, immunolabeled cells and live cells expressing fluorescently tagged cytoskeletal proteins. The implemented FiberScore program is used in order to recognize, segment, and quantify various structural parameters of the cytoskeleton, including total fiber-associated fluorescence, as well as fiber length and orientation. Furthermore, these parameters can be determined for different cytoskeletal proteins in the same sample tagged with multiple-fluorescent labels, and the results can be correlated with other cellular parameters.
Results: FiberScore was used here for the quantification of simultaneous changes in microtubule and actin filaments induced by the microtubule-disrupting drug nocodazole. Actin filaments, which are reported to respond reciprocally to microtubule disruption, are found to be affected by both immediate and delayed signals.
Conclusions: Analysis of the organization of fibers by the FiberScore algorithm allows quantification of the cytoskeletal signature of cells and offers reliable multiparametric functional assays for effects of drugs and other perturbations evaluated on a cell-by-cell basis. Cytometry Part A 54A:8–18, 2003. © 2003 Wiley-Liss, Inc.

Key terms: cytoskeleton; actin filaments; microtubules; quantitative microscopy; drug effects

Elucidation of the organization and dynamics of the cytoskeleton in cells is primarily based on data obtained from microscopic imaging. Since structural alterations in the cytoskeleton affect and reflect numerous physiological processes and states, such as the cell cycle, differentiation, adhesion, motility, and the activation of different signal transduction systems, the cytoskeletal signature offers an insight into the mechanisms underlying a wide spectrum of cellular processes.

High-resolution studies of the cytoskeleton have been carried out primarily by electron microscopy, yet for studies addressing the overall molecular organization, immunofluorescece microscopy is most commonly used. The light microscope with its lateral resolution of $\sim$0.2 μm can image the cytoskeletal fibers, and their cellular organization can be visualized in three dimensions by optical sectioning using wide-field microscopy followed by deconvolution or confocal laser scanning microscopy. This capacity has been extended from fixed-stained cells to live cells either microinjected with fluorescently labeled cytoskeletal molecules or expressing inherently fluorescent cytoskeletal fusion proteins. Live cell recording makes it possible to follow dynamic cellular processes and visualize directly structural changes in real time (1–3).

However, despite these important recent technological developments, quantitative studies of cytoskeleton assembly are mostly based on spectroscopic methods in cell extracted preparations. Immunofluorescence microscopy is still largely a qualitative, or semiquantitative, approach, with only few methods available for an accurate evaluation of the orientation, dimensions, and spatial distribution of specific cytoskeletal networks (4–9). In the absence of such quantitative tools, it is difficult to follow organizational changes of the cytoskeleton, determine the effects of drugs for dissection of cellular mechanisms and

Contract grant sponsor: Yad Abraham Center for Cancer Diagnosis and Therapy.
*Correspondence to: Zvi Kam, Department of Molecular Cell Biology, Weizmann Institute of Science, Rehovot 76100, Israel.
E-mail: zvi.kam@weizmann.ac.il
Published online in Wiley InterScience (www.interscience.wiley.com).
DOI: 10.1002/cyto.a.10053

for therapy (10,11), and study their involvement in various physiological processes or in specific regions within cells (such as at the leading lamella). One example, which might illustrate the need for a quantitative tool for the evaluation of cytoskeletal organization, is the elucidation of the mechanism underlying the cross talk between the microtubule and the microfilament networks. It has been shown that destruction of microtubules by drugs such as colcemid or nocodazole can stimulate the assembly of microfilament bundles and of focal adhesions (12). This effect was attributed to overall cell contraction induced by the drugs, which stimulates a Rho-A-dependent assembly of stress fibers (13,14), but other mechanisms may involve the molecular links between the two cytoskeletal networks (15).

In order to quantify specific structural features of microtubules and microfilaments, we developed image interpretation algorithms for segmentation of fiber-associated structures. We found that a standard binary threshold fails to exhaustively segment all fiber-associated structures in a cell, due to wide variations in intensity and background levels. Enhancement of rod-like patterns in immunofluorescent images by correlation with a series of rods at uniformly spaced rotation angles using fast Fourier transform (FFT) was proposed (16; Fig. 4 in Kam et al., 1992 [20]). For each angle, the difference between correlation with a rod and two flanking parallel rods is calculated to avoid high correlation values for regions of uniformly high intensity. The enhanced image is the maximum of these correlation differences among all rod angles. However, this algorithm was sensitive to fiber thickness. The present FiberScore algorithm applies a similar idea, but is extended and adapted for segmentation of fibers for a wide range of intensities and thicknesses. We have specifically applied the new algorithm to actin-based stress fibers and to microtubules. The former are largely straight (long persistence length), sometimes branched (with low-angle forks), and have variable thickness and intensity per unit length. Microtubules, on the other hand, form a wavy (shorter persistence length) network consisting of single fibers with variable packing densities. In some regions, usually around the cell center, the high density of microtubules hinders visibility of single fibers, while at the cell periphery the microtubule network is rather loose. The FiberScore algorithm takes into account these properties to recognize and quantify the total fluorescence intensity associated with the assembled fibers and evaluate morphological parameters such as fiber length, thickness, and orientation to characterize their organization. In this work we have applied FiberScore to determine the time- and dose-dependent differential effects of nocodazole on the actin and microtubule systems.

MATERIALS AND METHODS

Cells and Materials

Swiss 3T3 fibroblasts were cultured in Dulbecco Modified Eagle's Medium (DMEM), supplemented with 10% fetal calf serum (HyClone Laboratories, Logan, UT) in a humidified atmosphere of 7.5% CO_2 in air at 37°C. Cells were plated on fibronectin-coated coverslips (13-mm #1 Menzel Glass, Braunschweig, Germany) and cultured in serum-free medium for 24 h. These serum-starved cultures were incubated as indicated with nocodazole (methyl-(5-[2-thienylcarbonyl]-1H-benzimidazol-2-yl) carbamate, Sigma Chemical Co., St. Louis, MO) . Anti-tubulin antibodies (clone DM1A, T9026) were purchased from Sigma Immunochemicals (Rehovot, Israel). Rhodamine-labeled phalloidin was from Molecular Probes (Eugene, OR) or Sigma. FITC- and cy3-conjugated goat anti-mouse immunoglobulins were obtained from Jackson Laboratories (West Grove, PA). Alexa-488-conjugated goat anti-mouse antibody was from Molecular Probes.

For immunofluorescent labeling, cells were simultaneously fixed and permeabilized by brief (1 min) treatment with 0.25% Triton X-100 and 0.5% glutaraldehyde in cytoskeleton buffer (10 mM MES, 150 mM NaCl, 5 mM EGTA, 5 mM $MgCl_2$, and 5 mM glucose, pH 6.1) and then postfixed with 1% glutaraldehyde for 10 min, washed with PBS, and reduced in 1 mM sodium borohydride, to reduce autofluorescence. Coverslips were then incubated for 40 min with 10 μl of primary antibody droplets, mixed with 33 ngr/ml TRITC-conjugated phalloidin, washed three times with PBS, and incubated with the secondary antibodies for 40 min. After an additional three washes with PBS, the coverslips were mounted on glass slides in Elvanol (Mowiol 4-88, Hoechst, Frankfurt, Germany).

Swiss 3T3 cells, double-labeled for F-actin and tubulin, were subjected to fiber analysis. The stained cells were well spread, so that most of the fibers could be imaged in focus, and there was only a limited degree of out-of-focus blurring for fibers. Cells grown in serum-free medium were stimulated by the addition of serum and nocodazole at different concentrations (0.1, 0.3, 1, 3, and 10 μM) for 0–45 min. Cells were then immunofluorescently labeled and examined using a Zeiss Axiovert S100TV microscope (Oberkochen, Germany). Images were acquired with a cooled, scientific-grade CCD camera (Photometrics CH350 with Kodak KAF1400 chip) using the DeltaVision system (Applied Precision, Issaquah, WA). Pixel size was 6.0 μm and images were regularly binned ×2. There was no detectable degradation in fiber recognition by the binning process (see robustness to blurring in Results).

Partly enucleated CHO cells were prepared according to Chausovsky et al. (17). This treatment leads to variable loss of microtubule organization, allowing us to test the algorithm for wide variations in microtubule numbers and densities.

The FiberScore Algorithm

Typical fluorescent microscope images of cells labeled for actin and tubulin are shown in Figure 1a and e. The algorithm allows the reliable segmentation of these fibers, even for faint labeling and high background. We base this segmentation on the probability for each pixel neighborhood to belong to a fiber (fiber index). The fiber index image (Fig. 1b and f) is obtained by correlating regions around each pixel with synthetic fiber templates at differ-

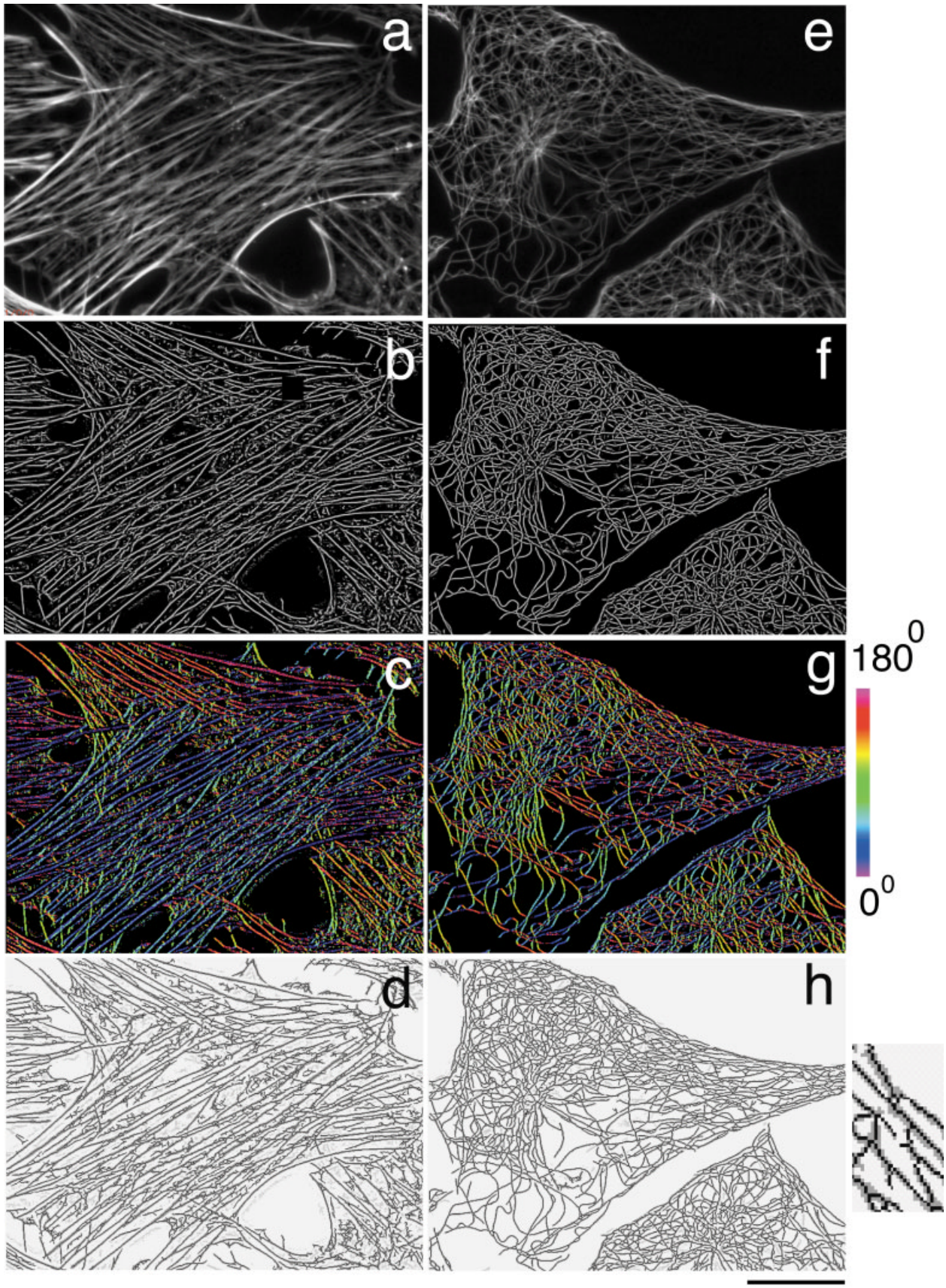

FIG. 1.

ent orientations and assigning for the central pixel the highest correlation coefficient among all orientations. In order to reduce the computational complexity, the two-dimensional correlation between the image and the fiber template was replaced by correlation with pairs of perpendicular lines. For these lines, the average intensity and standard deviation were also evaluated. The orientation of the line with the highest correlation coefficient is assigned for each pixel in the orientation image (Fig. 1c and g). Note the uniform orientation of the actin stress fibers, indicated by their uniform color in Figure 1c, compared to the nonuniform colors along the winding microtubules in Figure 1g. A binary mask is created where the fiber index correlation, average intensity, and standard deviation all exceed assigned thresholds (the pseudo-code for the algorithm is listed in Appendix I). This mask is used for segmentation of the original image and to calculate the fiber-associated parameters: fluorescence (total fiber score intensity) is summed in the mask after subtraction of background (see below and Appendix II). Morphological thinning of the mask (Fig. 1d and h) and connected component analysis is applied to evaluate the number of fibers, length, density, and polarity (Appendix III). Note that individual fibers are resolved even for regions with densely crossing fibers such as the actin bundles or the microtubules near their organizing center.

The algorithm was implemented as a module in the prism environment (18). The values obtained from the analysis (collectively referred to as cytoskeletal signature) allow a systematic comparison between cells following different treatments or during the performance of specific physiological functions, when combined with time-dependent dynamic imaging. This analysis can be carried out for cell populations, individual cells, or arbitrarily shaped regions of interest within a cell (see polygons enclosing individual cells in Figs. 2–4).

FIG. 1. **a** and **e:** Microscope images of Swiss 3T3 cells, fluorescently labeled with TRITC-phalloidin to visualize F-actin, and with anti-α-tubulin antibodies to display the microtubules. **b** and **f:** The fiber index mask images. For each pixel, the highest correlation between the original image and synthetic fibers at all orientations is assigned zeroing pixels that fail to exceed thresholds (see Appendix I). **c** and **g:** Fiber orientation image. The color table codes for the angle of the synthetic fiber for which the maximal correlation was obtained, indicating the direction of the fiber: 0° with the x-axis; purple, 45°; blue, 90°; green, 135°; red, 180°; and purple again. Stress fibers in (c) lie for this image in three major orientations, as opposed to the changing colors along a single microtubule path in (g). **d** and **h:** The binary mask, created from the fiber index image (gray), is thinned (black lines) (see enlargement), allowing evaluation of fiber length and intensity per unit length. Note the recognition of fibers with widely variable intensities and thicknesses. Note the identification of microtubule aster at the proximity of the organizing center. Light gray marks connected components shorter than a minimal length, which were excluded from the FiberScore quantifications. Scale bar = 20 μm.

	Total fiberscore intensity	Total length	Polarity	Intensity/length
Actin	2.2e8	7.9e4	.3	2.7e3
Microtubules	1.62e8	6.5e4	.1	2.5e3

Background Estimation

Quantitative fluorescence microscopy is based on the linear relationships between the fluorescent image intensity and the local concentration of the respective labeled epitope. This linearity is often perturbed by sample-derived or instrumental contributions grossly referred to as background. Cytoskeletal fiber labeling intensity is often comparable to the local background levels, and thus an accurate background evaluation and subtraction is essential.

However, background in biological specimens is usually nonuniform and its estimation is context dependent (based on prior knowledge of the signal patterns). Being diffuse, the spatial variation in the background level is usually smoother than the defined and structured fiber signal patterns. Background can thus be estimated locally around signal regions. This is the basis for the background estimation algorithms listed in Appendix II. We found that the rolling-ball method (19) provides the best results for quantitative fiber analysis. Other methods subtracted too much or too little background, depending on local fiber intensity and density. The FiberScore image is calculated by subtracting background from the original image and zeroing all nonfiber pixels (according to the binary mask generated by the FiberScore algorithm). Summation of total intensity for this masked background-subtracted image or inside any region of interest yields the total FiberScore intensity, which is proportional to the amount of labeled protein assembled into fibers.

Robustness of the FiberScore Algorithm

Total FiberScore intensities must be robust against nonideal image features frequently encountered in immunofluorescence microscopy of fixed or live cells. These include variable cell thickness producing different degrees of defocused details, nonuniform background levels (due to nonspecific labeling, fluorescence from cytoplasmic pools of nonassembled monomers, and autofluorescence), and low signal-to-noise ratios when exposure times are limited by bleach and phototoxicity. To test the robustness of the FiberScore algorithm, we used a series of simulations. We applied enucleation procedure to CHO cells (17) in order to prepare cell samples with large variations in fiber density and organization, and use their images for the different simulations (Figs. 2–4).

Noise is a salt-and-pepper effect in images due to photon-counting statistical uncertainty and detector electronic noise. It can be simulated by adding random values to the image (Fig. 2). For intensities above 10 photons, a noise with Gaussian distribution presents a good approximation to photon-counting Poisson statistics. The signal-to-noise ratio is determined by the relative variance, σ^2. For example, 12-bit intensity range (0–4095), and $\sigma^2 = 0.01$ means $\pm 4095\sqrt{0.01} = \pm 410$ added noise. The total FiberScore intensity did not change significantly by adding noise with values up to $\sigma^2 = 0.01$. The correlation coefficients between the total FiberScore intensities for pairs of images with and without added noise were >0.96. It is

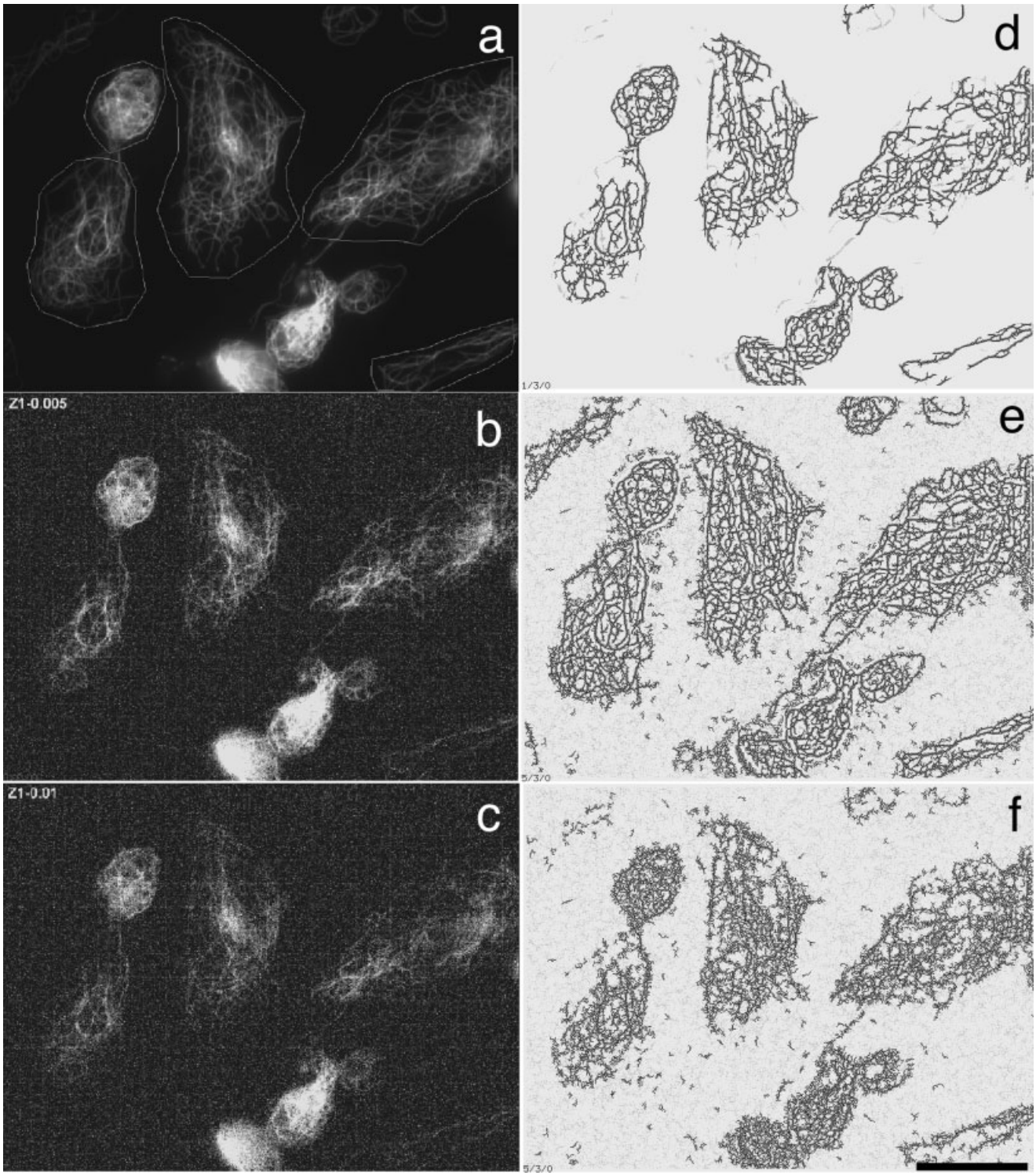

FIG. 2. Images of partly enucleated CHO cells displaying wide variability in microtubule densities, with added synthetic noise. **a:** The original image, with polygons allowing evaluation of total FiberScore intensity for each cell separately. **b** and **c:** The image with superimposed noise; mean value is zero and relative variance, $\sigma^2 = 0.005$ and 0.01, respectively. **d–f:** The corresponding thinned fiber masks. Note that although noise hinders fiber visualization, the algorithm depicts the fibers due to averaging of noise by the correlation with the synthetic rods, but also adds some new structures. Still, the total FiberScore intensity changed only slightly by adding noise (>.96 paired correlation coefficient between images with and without noise). This is explained by the small contributions of the added and weak fibers. Scale bar = 20 μm.

	Total fiberscore intensity	Total length	Polarity	Intensity/length
Original	4.9e7	2.0e4	.13	2.4e3
+0.005	5.0e7	2.2e4	.10	2.3e3
+0.01	5.2e7	2.6e4	.07	2.0e3

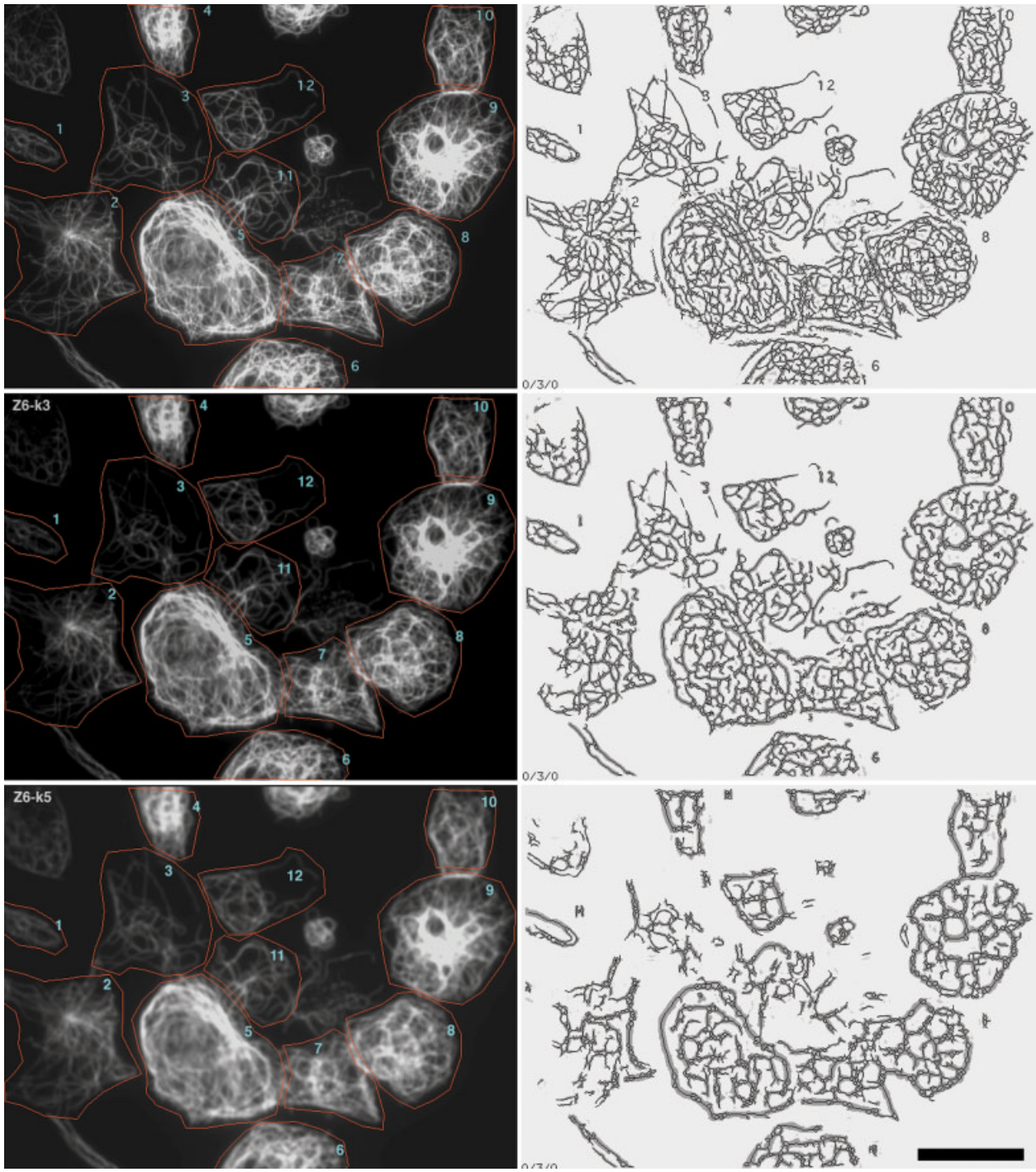

FIG. 3. Effect of defocusing simulated by smoothing filter. **a:** The original image. Numbered polygons define the scores for 12 individual cells in the image. **b** and **c:** The same image after applying low-pass filter with kernel sizes 3 and 5, respectively. **d** and **e:** The corresponding thinned FiberScore masks. Some loss of faint fibers is seen, yet the effect on the total FiberScore intensity is small. Scale bar = 20 μm. [Color figure can be viewed in the online issue, which is available at www.interscience.wiley.com.]

	Total fiberscore intensity	Total length	Polarity	Intensity/length
Original	5.9e7	2.4e3	.18	2.5e3
Kernel 3	5.8e7	2.3e3	.16	2.5e3
Kernel 5	5.6e7	2.0e3	.15	2.7e3

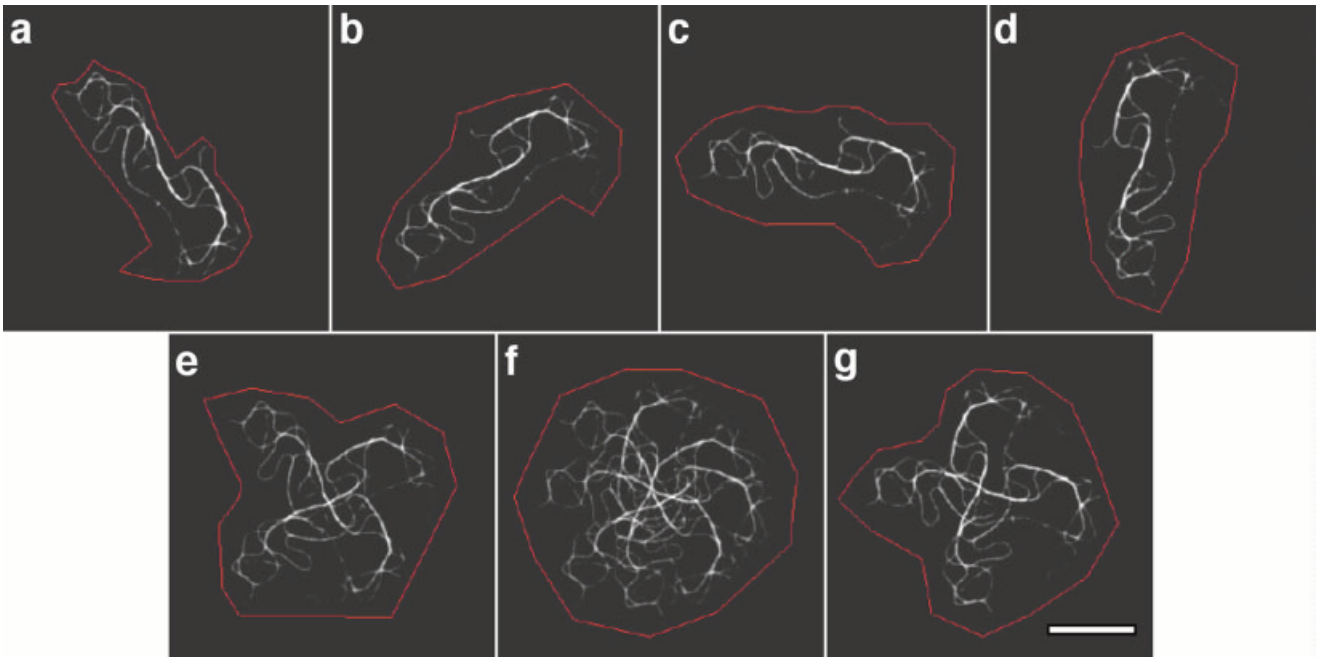

FIG. 4. A cell image rotated and stamped upon itself. **a:** The original image. **b–d:** Image rotated by 90°, 45°, and 135°, respectively. **e–g:** Sums of two (e and g) and four (f) rotated images. The polygons assign the region analyzed by FiberScore. Scale bar = 20 μm. [Color figure can be viewed in the online issue, which is available at www.interscience.wiley.com.]

	Fiberscore intensity	Total length	Polarity	Intensity/length
a. Original	2.2e6	9.4e2	.1	2.3e3
b. 90°	2.2e7	9.4e2	.1	2.3e3
c. 45°	2.2e7	9.4e2	.1	2.3e3
d. 135°	2.2e7	9.4e2	.1	2.3e3
e. 0° + 90°	4.3e7	1.8e3	.06	2.4e3
f. 0° + 45° + 90° + 135°	8.5e7	3.5e3	.04	2.4e3
g. 45° + 135°	4.3e7	1.8e3	.05	2.4e3

noteworthy that at high noise levels the visibility of the fibers is almost totally lost (see Fig. 2c).

Real images of cells display out-of-focus fibers above and below the set focal plane. Since change in focal plane will blur some fibers but better focus others, images acquired at a series of focal planes would not allow a controlled evaluation of the effect of blurring. We tested the effect of uniform defocusing by simulation, using smoothing filters with kernel sizes of 3 and 5 pixels, which correspond to the objective used here to defocus of 0.5 and 1 μm (Fig. 3). Smoothing, like physical defocusing, spread localized signals while preserving the total (integrated) intensity of the image. The correlation coefficients of total FiberScore intensities for all pairs of images without and with different degrees of blurring was above 0.95, indicating that the FiberScore algorithm is highly robust to a considerable degree of defocusing.

The dynamic range of an image (bit depth) presents the number of separable gray levels for pixel intensities. Although our images are acquired using 12-bit CCD (gray level between 0 and 4095), the actual dynamic range may be considerably lower for low-intensity features superimposed on high background or for short exposures, which is often essential in live cell work. For the simulation of low-bit images, a 12-bit image was transformed into images with 10, 8, 6, and 4 bits by integer number scaling. For example, total FiberScore intensity was 4.1e7 for the 12-bit image, 4.0e7 for the 8-bit image, and 3.8e7 for the corresponding 4-bit image, well corresponding to the digital truncation errors. The linear correlation coefficients between all pairs of total FiberScore intensities for the different bit resolutions were above 0.99 (images not shown).

Additional simulations were conducted in order to confirm that despite the discrete number of angles for the synthetic fiber templates, the FiberScore intensities did not depend on fiber orientation. Total FiberScore intensity changes due to computational rotation of an image (Fig. 4a–d) were below 5%. We also tested that intensities for crossing of overlapping fibers were additive. When a microtubule image of a cell was rotated and added onto itself for two orientations (Fig. 4e and g) and for four (Fig. 4f), total FiberScore intensities of the multiply stamped images were only slightly lower (<10%) than twice and four times the score for the original image, indicating the

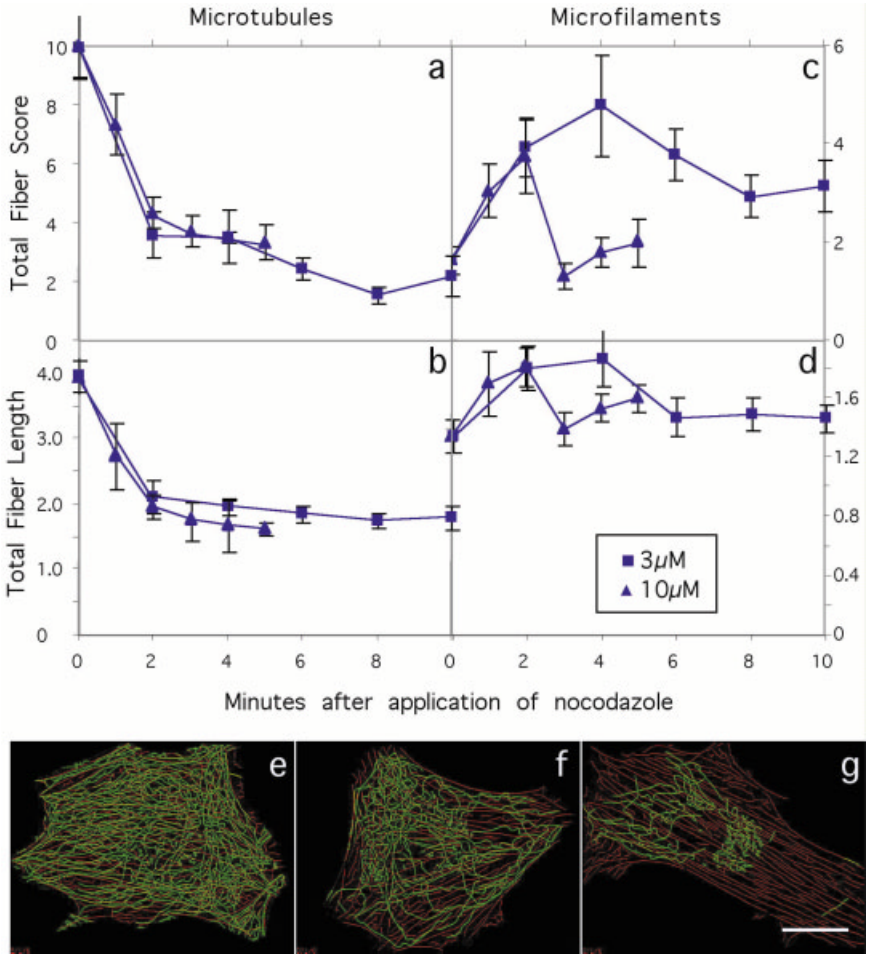

FIG. 5. Total FiberScore intensity (arbitrary units) and fiber length (pixels, 1 pixel = 0.133 μm) evaluated for microtubules and microfilament networks in double-labeled cells treated for a series of time duration with 3 and 10 μM nocodazole (squares and triangles, respectively) following starvation. Each data point presents the average and standard error for five analyzed cells. The disruption of the microtubule network is synchronized with enhancement of the actin network, mostly fiber bundle thickening, followed by delayed relaxation toward the initial score. Microtubule disruption and actin filaments' buildup dynamics are independent on nocodazole concentration, but the delayed relaxation of microfilaments toward the initial state is faster at 10 μM drug concentration. Three representative images displaying the FiberScore thinned actin (red) and microtubule fibers (green) are shown in (**e–g**) corresponding to 0, 1, and 4 min treatments in 3 μM nocodazole. Scale bar = 20 μm.

validity of this fiber quantification for high fiber density and crossings.

RESULTS AND DISCUSSION

Application of FiberScore for the Quantification of the Differential Effect of Nocodazole on Microtubules and Microfilaments

Serum-starved Swiss 3T3 cells, treated with the microtubule-disrupting drug nocodazole, were analyzed for their microtubule and actin stress fiber content as a function of drug concentration and duration of the treatment. For each drug concentration, five representative cells were analyzed and total FiberScore parameters and standard errors were computed. The higher the nocodazole concentration applied, the fewer intact microtubules that could be detected in the cells. However, cells treated with high concentrations of nocodazole displayed a textured, nonsmooth cytoplasmic background that most likely corresponds to tubulin aggregates or short fragments of microtubules. Since their intensity was comparable to that of long microtubules, they were initially scored as fibers. But since this texture produced in the analysis short and branched structures, they were distinguished from bona fide microtubules by conducting further morphological analysis of the length of the connected components in the thinned mask. After most of them were eliminated from the mask, the remaining value in the total FiberScore intensities establishes a baseline (about 2 in Fig. 5a) accounted by the remaining branched structures (see right of the nucleus in Fig. 5g).

Morphometric analysis allows the calculation of the FiberScore intensity per unit length, by dividing total FiberScore intensity by total fiber length. Microtubules are normally organized as single fibers with uniform thickness; therefore, FiberScore intensity per unit length is expected to be a constant. The variation in FiberScore intensity per unit length for images displaying a wide range of microtubule densities and background levels (after normalization for exposure time and excitation light intensity) was ±10%. This is a critical test for the validity of the linear relationship between intensities in the FiberScore images and the amount of fiber-assembled protein. The intensity per unit length values became less reliable for cells without intact microtubules though, due to the increasing number of the branched structures (see data in Fig. 5).

In previous studies it was shown that microtubule disruption induces the assembly of actin-containing stress fibers (12). In an attempt to quantify the reciprocal relationship between these two cytoskeletal systems, we have quantified the differential effect of nocodazole on actin and microtubules in the same cells. For that purpose, cells were treated for 0, 2, 4, 6, 8, and 10 min with 3 μM and for 0, 1, 2, 3, 4 and 5 min with 10 μM nocodazole. As shown in Figure 5, microtubules are almost totally disrupted within 2 min of treatment with the two concentrations of the drug. Total microtubule FiberScore intensity and total length kept being proportional, as expected (constant value for score per unit length). On the other hand, total actin FiberScore intensities in the same cells increased. Interestingtly, despite the fact that the changes in actin organization are presumably secondary to the destruction of microtubules, no delay was observed in actin assembly following application of nocodazole, suggesting that the microtubule-dependent reorganization of actin occurs at a subminute time frame. This is mainly due to thickening of existing fibers, since total actin scores about doubled, while length increased by only 25%. This effect was transient: total actin FiberScore intensities reached a peak after 2 and 4 min of treatment with 3 and 10 μM nocodazole, respectively, and returned to pretreatment values after 4 and 8 min, respectively. Interestingly, the rates of microtubule disruption and actin initial assembly were similar at 3 and 10 μM nocodazole concentrations, while the subsequent relaxation back toward initial values in the actin scores was faster at 10 μM then at 3 μM nocodazole. This suggests that following the initial, seemingly direct effect of microtubule disruption on actin fiber thickening (maybe via stress-related effects), there is a recovery that is slower for the high nocodazole concentration, probably due to indirect, delayed cellular responses.

In this work we applied FiberScore analysis to cell images in order to quantify the concerted changes in the organization of actin and microtubule cytoskeletal networks following perturbation. The analysis is robust against typical instrumental and biological problems in cell imaging experiments. The results demonstrate high degree of sensitivity to changes in the total cytoskeleton-assembled proteins as well as its morphology (polarity, fiber length, thickness). As opposed to biochemical and spectroscopic methods of fiber quantification, FiberScore analysis can be applied to small number of cells, is capable of simultaneous analysis of two or three different labels, and allows relation of the results to other cell-by-cell properties, notably transient expression of proteins suspected to affect cytoskeletal assembly or organization. The ability to identify fibers in high background is a necessary feature to apply this tool to GFP-tagged cytoskeletal proteins. Despite variability between individual cells, error bars for 5–10 cell averages are sufficiently small to detect 20–30% changes. Dynamic analysis of changes in live cell cytoskeletons is expected to reliably quantify even smaller changes by following a single cell in time. This is being pursued in our lab presently. The application of the analysis would therefore offer a powerful tool to study the effects of mutations, drugs, and environmental perturbations on cells, reflecting structural and signal transduction responses of the cell as presented by their cytoskeletal signature.

ACKNOWLEDGMENTS

We thank Prof. Adi Shamir for his interest in the problems and suggestion of inventive algorithms. Z.K. is the Israel Pollak Professor of Biophysics. B.G. holds the E. Neter Chair in Cell and Tumor Biology.

LITERATURE CITED

1. Yoon Y, Pitts K, McNiven M. Studying cytoskeletal dynamics in living cells using green fluorescent protein [Review]. Mol Biotechnol 2002; 21:241–250.
2. Ludin B, Matus A. GFP illuminates the cytoskeleton. Trends Cell Biol 1998;8:72–77.
3. Lippincott-Schwartz J, Snapp E, Kenworthy A. Studying protein dynamics in living cells. Nat Rev Mol Cell Biol 2001;2:444–455.
4. Howard TH, Oresajo CO. A method for quantifying F-actin in chemotactic peptide activated neutrophils: study of the effect of tBOC peptide. Cell Motil 1985;5:545–557.
5. Kohler M, Aufderheide M, Ramm D. Method for the description of differences in the filamentous structure of the cytoskeleton in cultured cells. Toxicol Lett 1994;72:33–42.
6. Schindelholz B, Reber BF. Quantitative estimation of F-actin in single growth cones. Methods 1999;18:487–492.
7. Shelden E, Wadsworth P. Observation and quantification of individual microtubule behavior in vivo: microtubule dynamics are cell-type specific. J Cell Biol 1993;120:935–945.
8. Rodionov V, Nadezhdina E, Peloquin J, Borisy G. Digital fluorescence microscopy of cell cytoplasts with and without the centrosome. Methods Cell Biol 2001;67:43–51.
9. Cramer LP, Briggs LJ, Dawe HR. Use of fluorescently labelled deoxyribonuclease I to spatially measure G-actin levels in migrating and non-migrating cells. Cell Motil Cytoskeleton 2002;51:27–38.
10. Jordan MA, Wilson L. Microtubules and actin filaments: dynamic targets for cancer chemotherapy. Curr Opin Cell Biol 1998;10:123–130.
11. Peterson JR, Mitchison TJ. Small molecules, big impact: a history of chemical inhibitors and the cytoskeleton. Chem Biol 2002;9:1275–1285.
12. Bershadsky A, Chausovsky A, Becker E, Lyubimova A, Geiger B. Involvement of microtubules in the control of adhesion-dependent signal transduction. Curr Biol 1996;6:1279–1289.
13. Small JV, Geiger B, Kaverina I, Bershadsky A. How do microtubules guide migrating cells? Nat Rev Mol Cell Biol 2002;12:957–964.
14. Rodionov VI, Hope AJ, Svitkina TM, Borisy GG. Functional coordination of microtubule-based and actin-based motility in melanophores. Curr Biol 1998;8:165–168.
15. Ren XD, Kiosses WB, Schwartz MA. Regulation of the small GTP binding protein Rho by cell adhesion and the cytoskeleton. EMBO J 1999;18:578–585.
16. Soferman Z. Computerized optical microscopy. PhD thesis, Weizmann Institute of Science, Rehovot, Israel, 1989.
17. Chausovsky A, Bershadsky A, Borisy GG. Cadherin-mediated regulation of microtubule dynamics. Nat Cell Biol 2000;2:797–804.
18. Chen H, Sedat JW, Agard DA. Manipulation, display, and analysis of three-dimensional biological images. In: Pawley JB, editor. Handbook of biological confocal microscopy. New York: Plenum Press; 1990. p 141–150.
19. Sternberg S. Biomedical image processing. Computer 1983;10:22–34.
20. Kam Z, Chen H, Sedat JW, Agard DA. Analysis of three-dimensional image data: display and feature tracking. In: Frank J, editor. Electron tomography: three-dimensional imaging with the transmission electron microscope. New York: Plenum Press; 1992. p 237–356.

APPENDIX I
The FiberScore Algorithm

A fiber is locally a narrow elongated structure (even though it may be tangled at a larger distance scale). A line of consecutive neighboring pixels along a fiber has

roughly uniform intensity (that equals the mean), with small standard deviations (SD), as opposed to a line of consecutive pixels perpendicular to a fiber, which has a large SD and a lower mean. Background pixels will display low SD and low mean values in all directions. We employ these features to assign fiber index to every pixel in an image.

Definitions

Let P(i,j) denote the intensity at point (i,j) of a two-dimensional image P. Let each pixel (i,j) be the center for 2K pixilated rod kernels at equally spaced rotation angles, θ_k:

$$\theta_k = k\Delta\theta_k; \quad \Delta\theta_k = \pi/(2K); \quad (k = 0, 1, 2 \ldots 2K - 1).$$

Let $[\delta_i(I,\theta_k), \delta_j(I,\theta_k)]$ (I = –L/2 . . . +L/2) be a list of L + 1 two-dimensional pixel displacements, which represent the one-dimensional nonzero pixilated line of elements in the (L + 1) × (L + 1) rod kernel for each θ_k:

$$[\delta_i(I, \theta_k), \delta_j(I, \theta_k)] = [\mathbf{I}, \mathbf{I}|tg(\theta_k)|],$$

$$if\ \theta_k < 45° \text{ or } \theta_k > 135°$$

$$= [\mathbf{I}|ctg(\theta_k)|, \mathbf{I}], \text{ if } 45° < \theta_k < 135°$$

The kernel intensities are weighted by a Gaussian profile along the rod length:

$$y_I = G[\delta_i(I, \theta_k), \delta_j(I, \theta_k)] = e^{-I'^2/2\omega},$$

$$\mathbf{I}' = 1/\max[|\sin(\theta_k)|, |\cos(\theta_k)|]$$

$$\bar{y} = \sum_{I=-L/2}^{+L/2} y_I/(L + 1)$$

For each pixel (i,j) and the neighboring image intensities along the rod:

$$x_I = P[i + \delta_i(I, \theta_k), j + \delta_j(I, \theta_k)]$$

a set of fiber values are calculated. The mean image intensity along the pixilated rod is

$$\boldsymbol{I}_{ij}(\theta_k) = \bar{x} = \sqrt{\sum_{I=-L/2}^{+L/2} x_I/(L + 1)},$$

the standard deviation (SD) of the intensities and the normalized standard deviation (NSD) are

$$\boldsymbol{SD}_{ij}(\theta_k) = \sqrt{\sum_{I=-L/2}^{+L/2} (x_I - \bar{x})^2/(L + 1)}$$

$$\boldsymbol{NSD}_{ij}(\theta_k) = SD_{ij}(\theta_k)/I_{ij}(\theta_k)$$

and the correlation coefficient of the Gaussian profile with the image intensities along the rod centered at point (i,j) is

$$\boldsymbol{C}_{ij}(\theta_k) = \sum_{I=-L/2}^{+L/2} (x_I - \bar{x}) \times (y_I - \bar{y})/\sqrt{\sum_{I=-L/2}^{+L/2} (x_I - \bar{x})^2 \sum_{I=-L/2}^{+L/2} (y_I - \bar{y})^2}.$$

Similarly, $\boldsymbol{I}_{ij}(\theta_k + \pi/2)$, $\boldsymbol{SD}_{ij}(\theta_K + \pi/2)$, $\boldsymbol{NSD}_{ij}(\theta_K + \pi/2)$ and $\boldsymbol{C}_{ij}(\theta_k + \pi/2)$, denote the corresponding fiber values for a perpendicular rod.

The Algorithm Pseudo-Code

The following algorithm computes:

Index (I,j) = Fiber index at (i,j), equals the highest correlation with the rotated rod kernel, and is zeroed if all fiber values do not exceed preset thresholds, thus creating fiber mask.

Orientation (i,j) = Orientation of the best correlated rod rotated about (i,j).

Mean (i,j) = Local average intensity along the rod at (i,j).

/* **Initialization loop** */
for each pixel (i,j)
{ **Index (i,j)** = 0; **Orientation (i,j)** = –100; **Mean (i,j)** = –1; }
/* **compute fiber correlation** */
for each orientation θ_k, between 0 and π/2 {
for each pixel (i, j) {
Calculate $C_{ij}(\theta_k)$, $I_{ij}(\theta_k)$, $NSD_{ij}(\theta_k)$, $C_{ij}(\theta_k + \pi/2)$, $I_{ij}(\theta_k + \pi/2)$, $NSD_{ij}(\theta_k + \pi/2)$
if $C_{ij}(\theta_k) > TC$ **and** $NSD_{ij}(\theta_k) > M$ **and** $NSD_{ij}(\theta_k)/NSD(\theta_k + \pi/2) > N$ **and** $I_{ij}(\theta_k + \pi/2) > T$
{ CMP = $C_{ij}(\theta_k)$ }
else { CMP = 0 }
if $C_{ij}(\theta_k + \pi/2) > TC$ **and** $NSD(\theta_k + \pi/2) > M$ **and** $NSD(\theta_k + \pi/2)/NSD_{ij}(\theta_k) > N$ **and** $I_{ij}(\theta_k) > T$
$\left\{CM = C_{ij}\left(\theta_k + \frac{\pi}{2}\right)\right\}$
else { CM = 0 }
if CM > CMP **and** CM > index (i,j)
{ **Index (i,j)** = CM; **Orientation (i,j)** = θ_k; **Mean (i,j)** = $\boldsymbol{I}_{ij}(\theta_k)$ }
else if CMP > CM **and** CMP > index (i,j)
{ **Index (i,j)** = CMP; **Orientation (i,j)** = $\theta_k + \pi/2$; **Mean (i,j)** = $\boldsymbol{I}_{ij}$ $(\theta_k + \pi/2)$ } } }

Typical Parameter Values

L = 6 = kernel size
K = 3 = angular resolution; $\Delta\theta_k = \pi/6$.
ω = 1 pixel
TC = 0.2 = threshold for correlation coefficient with a Gaussian profile
M = 0.01 = threshold for NSD

N = 1.1 = threshold for ratio of NSD between the perpendicular rods

T = threshold for background-subtracted intensity value for a fiber in the acquired image; value depends on the image, typically 100 for a 12-bit saturated image

APPENDIX II

Background Estimation Methods

Smoothing filter. Background is taken as the locally averaged intensity, calculated over a region larger than the typical size of the positively labeled sites. This is a good approximation if the total contribution of the signal within the region is small. Usually a square box region of size L × L allows application of a fast algorithm (complexity of the number of image pixels, N^2, not $L^2 \times N^2$) by updating only border pixels as the kernel is swept about the image (20).

Masked smoothing filter. As above, but the average excludes the segmented signal regions inside the mask. This is a good procedure, provided an objective mask exists. For critical applications, the mask created by segmentation algorithms can be dilated so that high signal pixels would not leak into the region where the background is estimated.

Local minimum value. The advantage of this estimate is its being independent on segmentation masks, and that background subtraction never produces negative values. However, the estimate is noise sensitive and tends to underestimate the background levels. Again, box kernels allow faster calculations.

Rolling ball. This method of background estimation can be described as the highest level to which a ball can be pushed up against the three-dimensional surface presenting the two-dimensional image and its intensity as height in the third dimension (17). The method is a kind of a smoothed minimum. Since the scale of intensities has different dimensionality from the pixel spacing, we actually slide an ellipsoid, rather than roll a ball. Our implementation also works for three-dimensional images.

Function fitting. Estimates a background function fitted to stretch between minima or flexing points. Usually linear or spline functions are used. This procedure may be necessary for small peaks superimposed on sloppy background.

APPENDIX III

Fiber Polarity and Length

Polarity, **D**, is defined as

$$\mathbf{D} = \sqrt{(\mathbf{D_x}^2 + \mathbf{D_y}^2)}$$

where

$\mathbf{D_x} = \Sigma$ **Mean (i,j)** $\cos(2\boldsymbol{\phi}\mathbf{ij})$/TotI; $\mathbf{D_y} = \Sigma$ **Mean(i,j)** $\sin(2\ \boldsymbol{\phi}\mathbf{ij})$/TotI

TotI = Σ **Mean(i,j)**

Mean angle is defined as

$\boldsymbol{\theta}_\mathbf{M} = 1/2 \arctan(\mathbf{D_y}/\mathbf{D_x})$

Total fiber length, **F**, is defined as

$\mathbf{F} = \Sigma\ 1/\max[|\cos(\boldsymbol{\phi}_{\mathbf{ij}})|, |\sin(\boldsymbol{\phi}_{\mathbf{ij}})|]$

where

$\boldsymbol{\phi}_{\mathbf{ij}}$ = **orientation(i,j)**, the direction of the best correlated rod for pixel (i,j).

For all sums, the Σ values are only for pixels (i, j) in the thinned fiber image.